JOURNAL OF COMPUTATIONAL PHYSICS 116, 343–358 (1995)

Discretisation and Multigrid Solution of Elliptic Equations with Mixed Derivative Terms and Strongly Discontinuous Coefficients

P. I. CRUMPTON, G. J. SHAW, AND A. F. WARE

Oxford University Computing Laboratory, Numerical Analysis Group, 11 Keble Road, Oxford, England OX1 3QD

Received June 7, 1993; revised March 7, 1994

This paper introduces a new conservative cell centred finite volume scheme for the accurate solution of elliptic diffusion equations with strongly varying coefficients. The discretisation is designed to model a wide range of heterogeneities and anisotropies, and in particular the case where the diffusivity is represented by a non-diagonal matrix, which may occur if the medium is anisotropic in a general direction. Such problems arise, for example, in oil reservoir simulation, when renormalisation techniques are used to model the reservoir geology. It is in this context that the method is described, although it is applicable to a far wider class of problems in heat conduction, electrostatics, and potential theory. The paper also describes the application of a multigrid scheme for efficient numerical solution of the algebraic equations derived using the new discretisation.

1. INTRODUCTION

Execution of the implicit stage of an implicit pressure explicit saturation (IMPES) reservoir simulation requires the discretisation and numerical solution of an elliptic equation for the pressure field in the reservoir. This equation is generally of the form

$$\nabla \cdot (K \nabla p) = f, \tag{1.1}$$

where K is the matrix of permeabilities. Heterogeneities in the porous medium are characterised by strong variation, by orders of magnitude, in the elements of K from one part of the region to another. Anisotropy occurs if the ratio between any two eigenvalues of K is large. In the case of a diagonal matrix K, in a two-dimensional region, this simply means that (1.1) is approximately a one-dimensional equation in one of the coordinate directions, which is simple to discretise in a conservative manner, but it requires consideration when choosing an appropriate iterative solution procedure. However, if renormalisation techniques [20] are used to model the geology of the reservoir, K may be a non-diagonal matrix and anisotropies can occur in general directions. This considerably complicates both the discretisation and numerical solution of the problem.

Much work has been done on the diagonal permeability case. Discretisation methods suitable for heterogeneous media may be derived by assuming piecewise constant permeabilities over grid blocks and taking a harmonic mean to obtain the permeability at a block interface [2]. The discrete algebraic system resulting from this discretisation may be solved relatively efficiently by iterative methods such as alternating direction implicit (ADI) [23], preconditioned conjugate gradients [13, 21, 14], Stone's strongly implicit procedure (SIP) [25], or ORTHOMIN [26]. More recently research has been published on the use of multigrid techniques for the solution of these problems. In [1, 4, 8, 7] the distinguishing feature of the multigrid is that grid transfer operators are based on the matrix coefficients, with Galerkin coarse grid matrices. This approach was extended to three-dimensional problems in [5, 9], in which plane relaxation was used as the smoothing method in order to cope with all the possible anisotropies. An alternative three-dimensional generalisation, based on semi-coarsening, appeared in [10]. By contrast Wesseling [27] used grid transfer operators which were independent of the matrix elements in order to derive a cell-centred finite volume multigrid scheme.

The aim of this paper is to consider the more general case of non-diagonal permeability matrices. The paper presents a conservative cell-centred discretisation, which reduces to the scheme mentioned above in the case of diagonal K. It also applies the multigrid scheme of [27] to the resulting algebraic system, showing that rapid mesh independent convergence rate may be obtained for problems of this type.

2. MODEL PROBLEM

Consider the following model problem:

$$Lp = \nabla \cdot (K \nabla p(\mathbf{x})) = f(\mathbf{x}), \quad \mathbf{x} = (x, y) \in \Omega \subset \mathbb{R}^2. \tag{2.1}$$

On the boundary $\delta\Omega$ of Ω, p will be specified on a non-empty subset $\delta\Omega_1$, and $(K \nabla p) \cdot \hat{\mathbf{n}}$ will be specified on $\delta\Omega_2 = \delta\Omega / \delta\Omega_1$. It is assumed that

$$K(\mathbf{x}) = \begin{pmatrix} K_{xx} & K_{xy} \\ K_{xy} & K_{yy} \end{pmatrix} \tag{2.2}$$

is a symmetric 2×2 matrix function of $\mathbf{x}$, which may be

0021-9991/95 $6.00

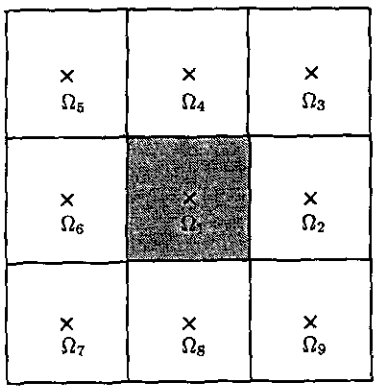

FIG. 1. Ordering of control volumes in nine point stencil. The shaded region is used to form the flux balance of (3.2).

discontinuous across internal boundaries of Ω. For (2.1) to be meaningful, discontinuities in the permeability matrix K must be accompanied by corresponding discontinuities in ∇p, such that $K\nabla p$ is a differentiable function of $\mathbf{x}$. It is further assumed that

$$K_{xx}K_{yy} > K_{xy}^2, \tag{2.3}$$

so that K is positive-definite and (2.1) is elliptic. It is important that the discretisation preserves the underlying ellipticity, in order that efficient multigrid methods may be developed for solution of the resulting algebraic equations.

3. CELL-CENTRED FINITE VOLUME DISCRETISATIONS

This section introduces a finite volume discretisation of the model problem (2.1). In order to motivate the more general method, which is derived in Section 3.3, we begin by deriving the standard method in the case of a diagonal permeability matrix and a uniform mesh. As will become apparent, the generalisation of this method to non-uniform meshes is not completely straightforward and has much in common with the generalisation to positive definite permeability matrices.

3.1. *Finite Volume Method on a Uniform Mesh*

Consider the case of (2.1) defined on the rectangular region $\Omega = (a, b) \times (c, d)$ and define the uniform mesh

$$\begin{aligned}\Omega^{(1)} = \{(x_i, y_j) : x_i = a + ih_x, y_j = c + jh_y,\\ i = 0, 1, ..., I, j = 0, 1, ..., J\},\end{aligned} \tag{3.1}$$

where $h_x = (b - a)/I$, $h_y = (d - c)/J$. The region Ω may then be subdivided into IJ elementary rectangular finite volumes, whose vertices are the nodes of $\Omega^{(1)}$. Each finite volume has side length h_x in the x direction and h_y in the y direction. Figure 1 shows nine such neighbouring cells denoted $\Omega_1, ..., \Omega_9$. The approximate solution of (2.1) is sought at the centre of each cell Ω_k and is denoted p_k. It will be assumed that K is smooth on each finite volume Ω_k, with average value K^k, although K may vary dramatically at cell interfaces. Integrating (2.1) over the cell Ω_1 gives

$$\int\int_{\Omega_1} \nabla \cdot (K\nabla p)\, dV = \oint_{\delta\Omega_1} (K\nabla p) \cdot \hat{\mathbf{n}}_1\, ds = \int\int_{\Omega_1} f\, dV, \tag{3.2}$$

where $\delta\Omega_1$ is the boundary contour of Ω_1 and $\hat{\mathbf{n}}_1$ is its unit outward normal. Using Green's theorem in the plane, Eq. (3.2) may then be written

$$\oint_{\delta\Omega_1} (K_{xx}p_x + K_{xy}p_y)\, dy - \oint_{\delta\Omega_1} (K_{xy}p_x + K_{yy}p_y)\, dx = h_x h_y f_1, \tag{3.3}$$

where

$$f_1 = \frac{1}{h_x h_y} \int\int_{\Omega_1} f\, dV. \tag{3.4}$$

The gradients in (3.3) cannot be evaluated using simple finite differences, since it is assumed that K may vary strongly between adjacent cells, leading to discontinuous gradients at cell boundaries. However, by exploiting continuity of both p and the normal flux on each interface, an accurate approximation may be obtained. This is described in the next section for a diagonal permeability matrix and in Section 3.3 for the more general case.

3.2. *Diagonal Permeability Matrix*

The method to be described here is in common usage and appears, for example, in Aziz and Settari [2], Stone [25], and Wesseling [28]. It is based on the flux balance (3.3) and leads to a five-point approximation to (2.1). When $K_{xy} \equiv 0$ the flux balance expressed in (3.3) reduces to

$$\oint_{\delta\Omega_1} K_{xx}p_x\, dy - K_{yy}p_y\, dx = h_x h_y f_1. \tag{3.5}$$

Consider the two adjacent cells Ω_1 and Ω_2 as depicted in Fig. 2. Since p is continuous across the interface between these two

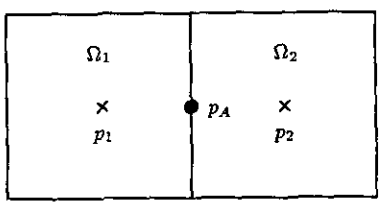

FIG. 2. Adjacent cells for the discretisation of Section 3.2; p_A is a fictitious state.

cells, it is reasonable to introduce a fictitious value p_A at the midpoint of this interface. Continuity of the normal flux at this point then gives the approximation

$$2K^1_{xx}\frac{(p_A - p_1)}{h_x} = 2K^2_{xx}\frac{(p_2 - p_A)}{h_x}, \tag{3.6}$$

which may be solved to give

$$p_A = \frac{K^1_{xx}p_1 + K^2_{xx}p_2}{(K^1_{xx} + K^2_{xx})}. \tag{3.7}$$

Note that the denominator cannot vanish since the fact that K^1 and K^2 are positive definite implies that their diagonal entries are positive. Substitution of (3.7) into either side of (3.6) then gives the flux on the interface as

$$K_{xx}p_x = \frac{2K^1_{xx}K^2_{xx}}{(K^1_{xx} + K^2_{xx})}\frac{(p_2 - p_1)}{h_x}, \tag{3.8}$$

which may be interpreted as a standard central difference with an effective permeability given by the harmonic mean of K^1_{xx} and K^2_{xx}.

Similar treatment of the remaining fluxes involved in (3.5), together with approximate integration by the midpoint rule allows (3.3) to be approximated by

$$\begin{aligned}&\frac{2K^1_{xx}K^2_{xx}}{(K^1_{xx} + K^2_{xx})}\frac{(p_2 - p_1)}{h_x^2} + \frac{2K^1_{xx}K^6_{xx}}{(K^1_{xx} + K^6_{xx})}\frac{(p_6 - p_1)}{h_x^2}\\ &+ \frac{2K^1_{yy}K^4_{yy}}{(K^1_{yy} + K^4_{yy})}\frac{(p_4 - p_1)}{h_y^2} + \frac{2K^1_{yy}K^8_{yy}}{(K^1_{yy} + K^8_{yy})}\frac{(p_8 - p_1)}{h_y^2} = f_1.\end{aligned} \tag{3.9}$$

Boundary conditions are simple to implement within the context of this method. If Dirichlet conditions are given on $\delta\Omega$ then the fictitious states there are assigned true values in place of approximations such as (3.7). If fluxes are given on the boundary these are used directly in place of approximations like (3.8).

Equation (3.9) is applied to each of the IJ control volumes in $\Omega^{(1)}$ and the resulting linear system is written as

$$L^{(1)}p^{(1)} = f^{(1)}. \tag{3.10}$$

Clearly $L^{(1)}$ is symmetric and, by virtue of the positive definiteness of K, it is also irreducibly diagonally dominant, with negative diagonal entries and non-negative off-diagonals. Consequently, it is negative definite and certain iterative methods, such as point Gauss–Seidel (PGS), are guaranteed to converge.

If flux boundary conditions are given everywhere on $\delta\Omega$ the solution of (2.1) is defined only to within an arbitrary additive constant. This manifests itself in the fact that $L^{(1)}$ is singular, having a constant eigenvector with zero eigenvalue. If this occurs the singularity may be removed by specifying p at some point on the boundary.

If K were constant throughout Ω the approximation (3.9) would reduce to the familiar central difference method

$$K_{xx}\frac{(p_2 - 2p_1 + p_6)}{h_x^2} + K_{yy}\frac{(p_4 - 2p_1 + p_8)}{h_y^2} = f_1, \tag{3.11}$$

which has a second-order truncation error

$$T_1\left[\frac{h_x^2}{12}K_{xx}\frac{\partial^4 p}{\partial x^4} + \frac{h_y^2}{12}K_{yy}\frac{\partial^4 p}{\partial y^4}\right]_{(x_1,y_1)}. \tag{3.12}$$

Note that the above approach leads to a five-point approximation. In the more general case $K_{xy} \neq 0$ the differential equation cannot be approximated to second-order accuracy using only five points. Note also that if either $K_{xy} \neq 0$ or the mesh is non-uniform, the directional derivative required to compute a flux on the interface is not, in general, aligned with the neighbouring approximate solutions. In these two cases a more general method is required. One possible approach is described in the next section.

3.3. *General Positive Definite Permeability Matrix*

The finite volume method of Section 3.1 requires the approximation of the term $(K\nabla p)\cdot\hat{\mathbf{n}}_1$ in Eq. (3.2) on cell interfaces. If either $K_{xy} \neq 0$ or the mesh is non-uniform, this term cannot be adequately approximated from only two neighbouring states. We will now describe a generalised approach for the case $K_{xy} \neq 0$. The same method is also applicable on a non-uniform mesh, with only minor modifications, which will be referred to in the forthcoming description.

The flux integrals in (3.2) along each side of the control volume Ω_1 will be approximated in two parts, each part being determined from the four states which surround its path of integration. The total flux integral for cell Ω_1 will therefore be a function of p_1 itself and the eight neighbouring states p_2, ..., p_9 as shown in Fig. 1. Consider the four neighbouring control volumes Ω_1, ..., Ω_4, which will be used to construct these approximate partial flux integrals, as shown in Fig. 3. By analogy with the method of the previous section fictitious states p_S, p_E, p_N, and p_W are introduced at the mid-sides of the interfaces between these cells. An additional fictitious state p_0 is also introduced at the intersection of all four cells. This is included in order to ensure continuity of the functional representation of p to be developed.

On each triangle shown in Fig. 3, p is approximated by a plane interpolant through its vertices. Thus, for example, for the triangle denoted α, the interpolant is given as

$$p_\alpha(x, y) = p_0 + 2x(p_S - p_1)/h_x + 2y(p_0 - p_S)/h_y, \tag{3.13}$$

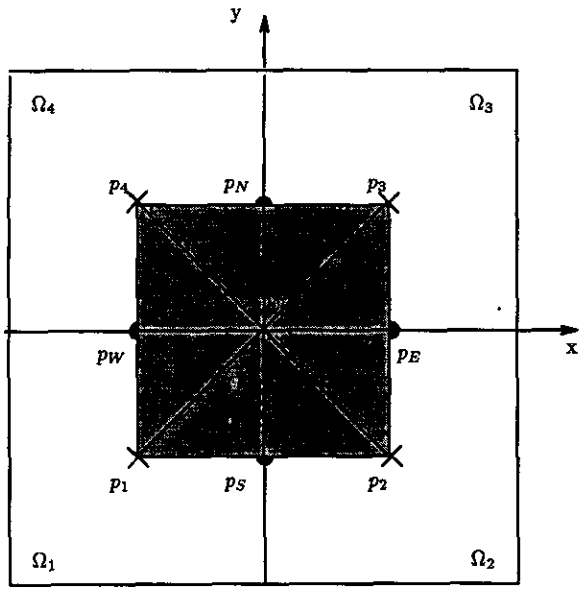

FIG. 3. Adjacent cells for the method of Section 3.3; p_0, p_S, p_E, p_N, and p_W are fictitious states. The shaded region is used to form the flux balance of (3.20) and is denoted Ω_0.

on a uniform mesh with local coordinate system centred at $\mathbf{x}_0$. A similar, although more complex, interpolant can clearly be obtained on a non-uniform mesh. Together, the plane interpolants on all eight triangles define a continuous, piecewise linear approximation to p, within the shaded region Ω_0 of Fig. 3.

Because of the linearity of the functional representation of p, the gradient vector is piecewise constant over Ω_0. Flux continuity conditions may now be easily imposed over interfaces between cells. Thus, for example, on the interface between Ω_1 and Ω_2, the first component of $K\,\nabla p$ is continuous, and this flux condition implies that

$$2K^1_{xx}\frac{(p_S - p_1)}{h_x} + 2K^1_{xy}\frac{(p_0 - p_S)}{h_y} = 2K^2_{xx}\frac{(p_2 - p_S)}{h_x} + 2K^2_{xy}\frac{(p_0 - p_S)}{h_y}, \tag{3.14}$$

which may be solved for p_S in terms of p_0 as

$$p_S = \frac{h_y(K^1_{xx}p_1 + K^2_{xx}p_2) + h_x(K^2_{xy} - K^1_{xy})p_0}{h_y(K^1_{xx} + K^2_{xx}) + h_x(K^2_{xy} - K^1_{xy})}, \tag{3.15}$$

provided the denominator does not vanish. This situation will be discussed at the end of this section. Note that if $K_{xy} \equiv 0$ then (3.15) reduces to

$$p_S = \frac{K^1_{xx}p_1 + K^2_{xx}p_2}{(K^1_{xx} + K^2_{xx})}, \tag{3.16}$$

and comparison with (3.7) shows that the method is equivalent to that of the previous section. Note also that if the mesh is non-uniform p_S is still a function only of p_0 and the given states p_1, p_2.

Flux continuity conditions similar to (3.15) may also be derived at the other three cell interfaces and lead to

$$p_E = \frac{h_x(K^2_{yy}p_2 + K^3_{yy}p_3) + h_y(K^2_{xy} - K^3_{xy})p_0}{h_x(K^2_{yy} + K^3_{yy}) + h_y(K^2_{xy} - K^3_{xy})}, \tag{3.17}$$

$$p_N = \frac{h_y(K^3_{xx}p_3 + K^4_{xx}p_4) + h_x(K^4_{xy} - K^3_{xy})p_0}{h_y(K^3_{xx} + K^4_{xx}) + h_x(K^4_{xy} - K^3_{xy})}, \tag{3.18}$$

$$p_W = \frac{h_x(K^4_{yy}p_4 + K^1_{yy}p_1) + h_y(K^4_{xy} - K^1_{xy})p_0}{h_x(K^4_{yy} + K^1_{yy}) + h_y(K^4_{xy} - K^1_{xy})}. \tag{3.19}$$

Given these definitions the piecewise linear interpolant is now continuous, with continuous normal fluxes at the interfaces. One more equation is required to uniquely define the functional representation. This is obtained by satisfying the integral form of the partial differential equation itself over the shaded region Ω_0. Thus, as in Section 3.1, the integral form is approximated by

$$\oint_{\delta\Omega_0}(K_{xx}p_x + K_{xy}p_y)\,dy - \oint_{\delta\Omega_0}(K_{xy}p_x + K_{yy}p_y)\,dx = h_x h_y f_0, \tag{3.20}$$

where

$$f_0 = (f_1 + f_2 + f_3 + f_4)/4. \tag{3.21}$$

Using the functional representation of p to evaluate the contour integral in (3.20) leads to the fifth equation,

$$C_0p_0 + C_Sp_S + C_Ep_E + C_Np_N + C_Wp_W + 2h_xh_y(K^1_{xy}p_1 - K^2_{xy}p_2 + K^3_{xy}p_3 - K^4_{xy}p_4) = h^2_xh^2_yf_0, \tag{3.22}$$

with

$$C_0 = -[h^2_y(K^1_{xx} + K^2_{xx} + K^3_{xx} + K^4_{xx}) + h^2_x(K^1_{yy} + K^2_{yy} + K^3_{yy} + K^4_{yy})] \tag{3.23}$$

and

$$\begin{aligned} C_S &= h^2_x(K^1_{yy} + K^2_{yy}) + h_xh_y(K^2_{xy} - K^1_{xy}) \\ C_E &= h^2_y(K^2_{xx} + K^3_{xx}) + h_xh_y(K^2_{xy} - K^3_{xy}) \\ C_N &= h^2_x(K^3_{yy} + K^4_{yy}) + h_xh_y(K^4_{xy} - K^3_{xy}) \\ C_W &= h^2_y(K^4_{xx} + K^1_{xx}) + h_xh_y(K^4_{xy} - K^1_{xy}). \end{aligned} \tag{3.24}$$

Equation (3.22), together with (3.15), (3.17)–(3.19), gives p_0 in terms of p_1, p_2, p_3, and p_4. This may then be substituted

back into (3.15), (3.17)–(3.19) in order to define all fictitious states and, hence, the functional representation of p in terms of these variables. Flux integral contributions from Ω_0 to (3.3) in the neighbouring cells may be computed from this representation. Namely,

$$\int_{-h_y/2}^{0} (K_{xx}p_x + K_{xy}p_y)\,dy = \frac{h_y}{2}\left[2K_{xx}^1\frac{(p_S - p_1)}{h_x} + 2K_{xy}^1\frac{(p_0 - p_S)}{h_y}\right] \quad (3.25)$$

$$\int_{0}^{h_x/2} (K_{xy}p_x + K_{yy}p_y)\,dx = \frac{h_x}{2}\left[2K_{xy}^2\frac{(p_E - p_0)}{h_x} + 2K_{yy}^2\frac{(p_E - p_2)}{h_y}\right] \quad (3.26)$$

$$\int_{0}^{h_y/2} (K_{xx}p_x + K_{xy}p_y)\,dy = \frac{h_y}{2}\left[2K_{xx}^6\frac{(p_6 - p_N)}{h_x} + 2K_{xy}^6\frac{(p_N - p_0)}{h_y}\right] \quad (3.27)$$

$$\int_{-h_x/2}^{0} (K_{xy}p_x + K_{yy}p_y)\,dx = \frac{h_x}{2}\left[2K_{xy}^4\frac{(p_0 - p_W)}{h_x} + 2K_{yy}^4\frac{(p_4 - p_W)}{h_y}\right] \quad (3.28)$$

These partial integrals are then distributed to the relevant equations, based at Ω_1, Ω_2, Ω_3, and Ω_4, with appropriate signs. Note that if $K_{xy} \equiv 0$ this discretisation becomes independent of p_0 and reduces to that of (3.9).

Boundary conditions are again easily implemented. If Dirichlet conditions are given then all the fictitious states on the boundary are assigned their true values and the remaining states are defined to satisfy the flux continuity conditions. If fluxes are given on $\delta\Omega$ the flux derived from the functional representation is set to its true value.

As mentioned above, the derivation of the scheme outlined in this section does not hold if any of the denominators in (3.15), (3.17)–(3.19) vanish. Unfortunately positive definiteness of the permeability matrices is no guarantee that this cannot occur. However, should these denominators vanish it does not necessarily follow that the system of five equations defining p_S, p_E, p_N, p_W, and p_0 is singular. It may merely indicate that the system requires pivoting. By writing (3.14) and its equivalent for p_E, p_N, and p_W, together with (3.22) as a system of five linear equations, the solution may still be sought by Gaussian elimination with partial pivoting. Since it is almost essential to store the entries of $L^{(1)}$ if any iterative solution technique is to prove successful, this Gaussian elimination is part of the preprocessing and has to be performed once only. Consequently its expense is not prohibitive. In the numerical experiments conducted below the fictitious states were always obtained by Gaussian elimination, regardless of whether the denominators vanished or not. The cpu times were found to be very strongly dominated by the cost of the iterations, rather than the preprocessing.

4. PROPERTIES OF THE DISCRETISATION

Having derived the cell-centred finite volume discretisation of the previous section it would be desirable to analyse the accuracy of the method and the convergence behaviour of certain iterative schemes when applied to its solution. In particular, it would be advantageous to estimate the rate of convergence attainable by the multigrid methods to be developed in Section 5. This is generally achieved by means of Fourier analysis, which is applicable only in the case of constant permeability and a uniform mesh. Since the main interest of this paper lies in problems with discontinuous coefficients such an analysis can only be of limited benefit. However, it is still important to consider the Fourier analysis, as the stability of the method for constant coefficients is clearly necessary for stability in the more general case.

This section is therefore devoted to analysis of the constant coefficient discretisation, which is outlined in Section 4.1. Its accuracy is discussed in Section 4.2, and discrete ellipticity is discussed in Section 4.3. This latter property is crucial for the development of the efficient multigrid solution procedures to be outlined in Section 5.

4.1. *The Special Case of Constant Permeability*

If K is constant and the mesh is uniform, with $h_x = h = h_y$, the discrete approximations derived in the previous section simplify considerably. The fictitious states are defined by

$$\begin{aligned} p_S &= \tfrac{1}{2}(p_1 + p_2), \quad p_E = \tfrac{1}{2}(p_2 + p_3), \\ p_N &= \tfrac{1}{2}(p_3 + p_4), \quad p_W = \tfrac{1}{2}(p_4 + p_1), \end{aligned} \quad (4.1)$$

and

$$p_0 = \tfrac{1}{4}(p_1 + p_2 + p_3 + p_4) + \frac{K_{xy}}{2(K_{xx} + K_{yy})}(p_1 - p_2 + p_3 - p_4) - \frac{h^2 f_0}{4(K_{xx} + K_{yy})}. \quad (4.2)$$

The resulting discrete approximation to (2.1) is then

$$\frac{K_{xx}}{h^2}(p_2 - 2p_1 + p_6) + \frac{K_{yy}}{h^2}(p_4 - 2p_1 + p_8) + \frac{K_{xy}}{2h^2}(p_3 - p_5 + p_7 - p_9) + \frac{(K_{xy})^2}{h^2(K_{xx} + K_{yy})} \quad (4.3)$$

$$[4p_1 - 2(p_2 + p_4 + p_6 + p_8) + p_3 + p_5 + p_7 + p_9] = f_1 + \frac{K_{xy}}{8(K_{xx} + K_{yy})}(f_3 - f_5 + f_7 - f_9),$$

which is the standard second-order nine-point approximation to (2.1), augmented by an additional term, with stencil

$$\frac{(K_{xy})^2}{h^2(K_{xx} + K_{yy})}\begin{bmatrix} 1 & -2 & 1 \\ -2 & 4 & -2 \\ 1 & -2 & 1 \end{bmatrix}, \tag{4.4}$$

together with a weighted averaging of the source terms. The extra term (4.4) corresponds to a mixed fourth derivative. Its effect on the stability of the scheme will be investigated in Section 4.3. As an indication of the effect of this additional term on the stencil, consider the parabolic problem

$$\frac{\partial^2 p}{\partial x^2} + 2\frac{\partial^2 p}{\partial x \partial y} + \frac{\partial^2 p}{\partial y^2} = 0, \tag{4.5}$$

for which

$$K = \begin{pmatrix} 1 & 1 \\ 1 & 1 \end{pmatrix}. \tag{4.6}$$

This states that the second derivative of p is zero along the lines $y = x + c$, for arbitrary c, which are diagonals of a uniform mesh. The standard nine-point approximation leads to the stencil

$$\frac{1}{2h^2}\begin{bmatrix} -1 & 2 & 1 \\ 2 & -8 & 2 \\ 1 & 2 & -1 \end{bmatrix}, \tag{4.7}$$

which, on the addition of the extra term becomes

$$\frac{1}{h^2}\begin{bmatrix} 0 & 0 & 1 \\ 0 & -2 & 0 \\ 1 & 0 & 0 \end{bmatrix}. \tag{4.8}$$

The latter stencil is diagonally dominant and corresponds to a standard central difference along the relevant diagonal of the mesh.

4.2. *Accuracy*

The truncation error associated with discrete equation (4.3) is

$$T_1 = \frac{h^2}{12}\left[K_{xx}\frac{\partial^4 p}{\partial x^4} + 4K_{xy}\left(\frac{\partial^4 p}{\partial x^3 \partial y} + \frac{\partial^4 p}{\partial x \partial y^3}\right) + K_{yy}\frac{\partial^4 p}{\partial y^4}\right]_{(x_1, y_1)} - \frac{h^2 K_{xy}}{2(K_{xx} + K_{yy})}\left[K_{xx}\frac{\partial^4 p}{\partial x^3 \partial y} + K_{yy}\frac{\partial^4 p}{\partial x \partial y^3}\right]_{(x_1, y_1)}, \tag{4.9}$$

and is therefore second order in regions where p is sufficiently smooth. The additional term (4.4) does not affect the order of the truncation error since it approximates the second-order term

$$\frac{h^2(K_{xy})^2}{(K_{xx} + K_{yy})}\frac{\partial^4 p}{\partial x^2 \partial y^2}\bigg|_{(x_1, y_1)}. \tag{4.10}$$

As for the method of Section 3.2, the matrix $L^{(1)}$ is symmetric, with negative diagonal entries. In fact, the diagonal elements are given by

$$C_1 = \frac{4(K_{xy})^2 - 2(K_{xx} + K_{yy})^2}{h^2(K_{xx} + K_{yy})} < -2\frac{[(K_{xx})^2 + (K_{yy})^2]}{h^2(K_{xx} + K_{yy})}, \tag{4.11}$$

by virtue of the positive definiteness of K. However, it is not possible in general to show that $L^{(1)}$ is diagonally dominant, which precludes the use of a maximum principle to bound the global error.

4.3. *Discrete Ellipticity*

The Fourier symbol of $L^{(1)}$ in the constant coefficient case is

$$L^{(1)}(\theta_x, \theta_y) = K_{xx}(1 - \cos\theta_x) + K_{yy}(1 - \cos\theta_y) + K_{xy}\sin\theta_x \sin\theta_y - \frac{2(K_{xy})^2}{(K_{xx} + K_{yy})}(1 - \cos\theta_x)(1 - \cos\theta_y). \tag{4.12}$$

Without the additional term (4.4) the symbol is merely

$$L^{(1)}(\theta_x, \theta_y) = K_{xx}(1 - \cos\theta_x) + K_{yy}(1 - \cos\theta_y) + K_{xy}\sin\theta_x \sin\theta_y. \tag{4.13}$$

In the case of (4.13) it is straightforward to show that $L^{(1)}(\theta_x, \theta_y) \geq 0$ and vanishes only at the origin, provided K is positive definite. This means that the standard nine-point scheme is discretely elliptic, which has important consequences on the existence of smoothing methods for multigrid.

We shall prove a similar result for the symbol (4.12). If we write s_x (respectively s_y, c_x, c_y) for $\sin(\theta_x/2)$ (respectively $\sin(\theta_y/2)$, $\cos(\theta_x/2)$, $\cos(\theta_y/2)$), then the symbol (4.12) may be expanded in the form

$$L^{(1)}(\theta_x, \theta_y) = \left(\frac{2}{K_{xx} + K_{yy}}\right)A(\theta_x, \theta_y), \tag{4.14}$$

where

$$A(\theta_x, \theta_y) = (K_{xx}s_x)^2 + (K_{yy}s_y)^2 + K_{xx}K_{yy}(s_x^2 + s_y^2) - 4(K_{xy}s_xs_y)^2 + 2K_{xy}(K_{xx} + K_{yy})s_xc_xs_yc_y. \tag{4.15}$$

The algebra is considerably simplified if we write

$$\alpha = \frac{|K_{xy}|}{(K_{xx}K_{yy})^{1/2}},$$

where, as a consequence of ellipticity, $\alpha < 1$. The final term in A may be bounded by use of Young's inequality:

$$\begin{aligned} 2(K_{xx} + K_{yy})|K_{xy}s_xc_xs_yc_y| &= 2\alpha(K_{xx} + K_{yy})|(K_{xx}K_{yy})^{1/2}s_xc_xs_yc_y| \\ &\le \alpha(K_{xx} + K_{yy})(s_x^2c_x^2K_{xx} + s_y^2c_y^2K_{yy}). \end{aligned}$$

Substituting into the expression for A and expanding further we obtain

$$\begin{aligned} &A(\theta_x, \theta_y) \\ &\quad \ge (K_{xx}s_x)^2 + (K_{yy}s_y)^2 + K_{xx}K_{yy}(s_x^2 + s_y^2) - 4\alpha^2K_{xx}K_{yy}s_x^2s_y^2 \\ &\qquad - \alpha(K_{xx} + K_{yy})(K_{xx}s_x^2 + K_{yy}s_y^2 - K_{xx}s_x^4 - K_{yy}s_y^4) \\ &\quad = (1 - \alpha)((K_{xx}s_x)^2 + (K_{yy}s_y)^2 + K_{xx}K_{yy}(s_x^2 + s_y^2)) \\ &\qquad + \alpha((K_{xx}s_x^2)^2 + (K_{yy}s_y^2)^2 + K_{xx}K_{yy}(s_x^4 + s_y^4 - 4\alpha s_x^2s_y^2)) \\ &\quad \ge (1 - \alpha)(K_{xx}s_x^2 + K_{yy}s_y^2)^2 \\ &\qquad + \alpha((K_{xx}s_x^2 - K_{yy}s_y^2)^2 + K_{xx}K_{yy}(s_x^2 - s_y^2)^2), \end{aligned}$$

where we have made further use of Young's inequality. Discrete ellipticity now follows.

5. CELL-CENTRED MULTIGRID METHOD

The system of discrete equations

$$L^{(1)}p^{(1)} = f^{(1)}, \tag{5.1}$$

derived using the method of Section 3.3, is sparse, linear, and banded, and it is amenable to solution by iterative techniques such as alternating line Gauss–Seidel [30], incomplete LU decomposition [21], preconditioned conjugate gradients [14], or multigrid [6, 19]. Of these, multigrid is potentially the most efficient. Ideally, it is optimally fast, obtaining mesh independent convergence rates. Thus multigrid requires the same number of iterations to achieve a given reduction in the residual norm on any mesh, whereas the other methods all require more as the mesh is refined.

The multigrid scheme to be described here is based on that of Wesseling [27], which was designed to solve the discrete systems arising from the cell-centred method for diagonal permeability matrices presented in Section 3.2. That scheme is highly efficient for these problems, and very little modification is required in the more general case.

5.1. *Multigrid Algorithm*

Multigrid uses a sequence of meshes $\Omega^{(k)}$, $k = 2, ..., m$, of increasing coarseness, to accelerate the convergence of a basic iterative procedure, such as those mentioned above, on the original mesh $\Omega^{(1)}$. The coarser meshes are obtained by collecting four adjacent fine-grid control volumes together to define a single coarse-grid control volume. Thus if

$$\Omega^{(1)} = \{(x_i, y_j) : x_i = a + ih_x^{(1)}, y_j = c + jh_y^{(1)}, \quad i = 0, 1, ..., I, j = 0, 1, ..., J\} \tag{5.2}$$

with $h_x^{(1)} = (b - a)/I$, $h_y^{(1)} = (d - c)/J$ defines the nodes of the original mesh, as in (3.1), the coarser meshes are given by

$$\Omega^{(k)} = \{(x_i, u_j) : x_i = a + ih_x^{(k)}, y_j = c + jh_y^{(k)}, \quad i = 0, 1, ..., I/2^{(k-1)}, j = 0, 1, ..., J/2^{(k-1)}\}, \tag{5.3}$$

where $h_x^{(k)} = 2^{(k-1)}(b - a)/I$, $h_y^{(k)} = 2^{(k-1)}(d - c)/J$. The coarsening process stops at $\Omega^{(m)}$ if $\Omega^{(m+1)}$ is not well defined. This occurs when either $I/2^m$ or $J/2^m$ is not an integer. The convergence rate of the multigrid algorithm is enhanced by the addition of more coarse meshes, and so it is desirable to maximise m by suitable choice of I and J. However, this restriction on the choice of I, J may be circumvented at the cost of complicating the algorithm somewhat. Alternatively, if zero flux boundary conditions are given, the mesh may be extended to a more convenient dimension by adding cells around the boundary which have $K = 0$.

Multigrid achieves its mesh independent convergence rates by combining two algorithms with complementary properties. The basic iterative procedure is generally efficient at damping high frequency error components, but not at smooth modes. For this reason it is referred to as a smoother in the context of multigrid methods. It is combined with a coarse-grid correction step, which uses the coarser meshes to approximately eliminate the smooth low frequency error modes. If this is achieved sufficiently well the convergence of the process is dominated by the rate at which the smoother damps the high frequency modes. This can be accurately analysed by Fourier analysis in the case of constant K and a uniform mesh.

Assume that on each mesh $\Omega^{(k)}$ there is a discrete approximation

$$L^{(k)}p^{(k)} = f^{(k)}, \tag{5.4}$$

to (2.1). Assume also that there exists a restriction operator R_k^{k+1} mapping the unknowns of a fine mesh $\Omega^{(k)}$ to those of a

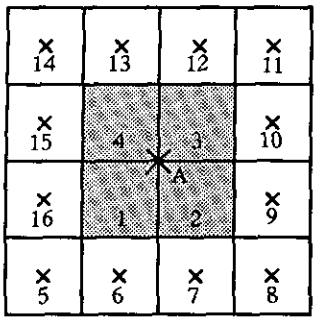

FIG. 4. Illustration of grid transfer operators. The shaded region represents the control volume surrounding a coarse grid point.

coarser mesh $\Omega^{(k+1)}$, and a prolongation operator P_{k+1}^k mapping the unknowns of $\Omega^{(k+1)}$ to $\Omega^{(k)}$. An iteration of multigrid applied to (5.4) on $\Omega^{(k)}$ is as follows:

- do ν_1 sweeps of a smoothing procedure on $\Omega^{(k)}$, starting from $\tilde{p}^{(k)}$ and producing an approximate solution $\bar{p}^{(k)}$ of $L^{(k)}p^{(k)} = f^{(k)}$
- form the residual: $r^{(k)} = f^{(k)} - L^{(k)}\bar{p}^{(k)}$
- restrict the residual to the right-hand side on coarser mesh $\Omega^{(k+1)}$: $f^{(k+1)} = R_k^{k+1} r^{(k)}$
- if $k = m - 1$, solve $L^{(m)}\tilde{p}^{(m)} = f^{(m)}$ directly; otherwise do γ iterations of multigrid on $\Omega^{(k+1)}$, starting from $p^{(k+1)} = 0$ and resulting in an approximate solution $\tilde{p}^{(k+1)}$ of $L^{(k+1)}p^{(k+1)} = f^{(k+1)}$
- prolong the correction $\tilde{p}^{(k+1)}$ to $\Omega^{(k)}$ and add to the current fine-grid solution: $\hat{p}^{(k)} = \bar{p}^{(k)} + P_{k+1}^k \tilde{p}^{(k+1)}$
- do ν_2 sweeps of a smoothing procedure on $\Omega^{(k)}$, starting from $\hat{p}^{(k)}$ and producing an approximate solution $\tilde{p}^{(k)}$ of $L^{(k)}p^{(k)} = f^{(k)}$

Note that the algorithm is recursive, the coarse grid problem being solved itself by the multigrid, using a still coarser grid. In order to fully define the algorithm, it is necessary to choose ν_1, ν_2, γ, the smoother, the grid transfer operators R_k^{k+1}, P_{k+1}^k, and the coarse-grid operators $L^{k+1}, k = 1, 2, ..., m - 1$. Typically $\nu_1 = 1$, $\nu_2 = 1$, and $\gamma = 1$ are chosen, and these are the values used throughout this paper. The grid transfer and coarse-grid operators are outlined in the next section. Finally, Section 5.3 discusses the choice of the smoothing scheme.

5.2. *Grid Transfer and Coarse Grid Operators*

The grid transfer and coarse-grid operators used in this paper are those of Wesseling [27], which were shown to be suitable for problems with discontinuous diagonal permeability matrices, discretised using the cell-centred finite volume method of Section 3.2. The prolongation is simple. A coarse-grid state to be prolonged is simply distributed to each of the fine-grid cells that are contained in its control volume. Thus, with reference to Fig. 4, the prolongation of the coarse grid state p_A gives rise to the fine grid states:

$$p_1 := p_A, \quad p_2 := p_A, \quad p_3 := p_A, \quad p_4 := p_A. \tag{5.5}$$

This may be represented in stencil form as

$$P_{k+1}^k = \begin{bmatrix} 1 & 1 \\ 1 & 1 \end{bmatrix}. \tag{5.6}$$

This prolongation is exact only for piecewise-constant coarse-grid functions and is said to be of order $\mathbb{O}_P = 1$ [27].

The restriction R_k^{k+1} from the fine grid Ω_k to the coarse grid Ω_{k+1} is taken as the adjoint of a linear interpolation operator. The coarse-grid state p_A is defined to be

$$\begin{aligned} p_A = \tfrac{1}{16}\{&3(p_2 + p_4) + 2(p_1 + p_3) \\ &+ p_7 + p_8 + p_9 + p_{13} + p_{14} + p_{15}\}, \end{aligned} \tag{5.7}$$

or in stencil form,

$$R_k^{k+1} = \frac{1}{16}\begin{bmatrix} 1 & 1 & & \\ 1 & 3 & 2 & \\ & 2 & 3 & 1 \\ & & 1 & 1 \end{bmatrix}. \tag{5.8}$$

The interpolation rule to which this restriction is adjoint is exact for piecewise linear coarse-grid functions, and the restriction is therefore deemed to be of order $\mathbb{O}_R = 2$. for the multigrid method to be successful it is necessary that

$$\mathbb{O}_P + \mathbb{O}_R > \mathbb{O}_E, \tag{5.9}$$

where $\mathbb{O}_E$ is the order of the differential equation [6]. In the case of (2.1) $\mathbb{O}_E = 2$ and (5.9) holds. The simpler restriction

$$R_k^{k+1} = \frac{1}{4}\begin{bmatrix} 1 & 1 \\ 1 & 1 \end{bmatrix}, \tag{5.10}$$

which is the adjoint of (5.6) only has $\mathbb{O}_R = 1$ and violates (5.9).

The definition of a linear interpolation from Ω_{k+1} to Ω_k is non-unique, and consequently, (5.6) is not the only adjoint second-order restriction. For example,

$$R_k^{k+1} = \frac{1}{16}\begin{bmatrix} 1 & & & 1 \\ & 3 & 3 & \\ & 3 & 3 & \\ 1 & & & 1 \end{bmatrix} \tag{5.11}$$

is a second-order restriction adjoint to a more symmetric linear

interpolation rule. Inequality (5.9) would still hold if this restriction were used in place of (5.6).

Near boundaries the prolongation (5.6) requires no modification, but the restrictions (5.8) and (5.11) involve fine grid states lying outside the domain; the appropriate operators are obtained by approximating these by linear extrapolation using the boundary data.

The coarse-grid operator $L^{(k+1)}$ is defined using the Galerkin approach. Thus

$$L^{(k+1)} = R_k^{k+1} L^{(k)} P_{k+1}^k. \tag{5.12}$$

This prescription of $L^{(k+1)}$ ensures that the coarse-grid correction iteration matrix has zero eigenvalues for every eigenvector lying in the range of P_{k+1}^k. Such eigenvectors are generally smooth, so that the coarse-grid correction damps smooth modes, leaving the high frequency error components to be reduced by the smoothing method. If $L^{(k)}$ is a nine-point operator, then $L^{(k+1)}$ defined by (5.12), using any of the prolongations or restrictions described above, is also a nine-point operator. If the restriction and prolongation are adjoint then a positive definite fine-grid matrix $L^{(k)}$ gives rise to a positive definite coarse-grid matrix $L^{(k+1)}$. This would suggest advantages to using (5.6), together with (5.10). However, as mentioned above this choice violates (5.9) and the multigrid method is not expected to work. Another possibility might be to use (5.8) as the restriction, with the prolongation defined as its linear interpolation adjoint. Then (5.9) is satisfied since $\mathbb{O}_R + \mathbb{O}_P = 4$, and the Galerkin definition (5.12) preserves positive definiteness. The disadvantage here is that this choice of grid transfer operators leads to an extended coarse-grid stencil of more than nine points. The results presented in this paper are therefore all obtained using the definitions (5.6), (5.8), and (5.12), which are precisely the choices made by Wesseling [27].

5.3. *Smoothing Methods*

The standard iterative procedure used in the multigrid algorithm may be chosen from a host of possible schemes [15, 3]. These include the following:

- Jacobi and Gauss–Seidel schemes, possibly using a relaxation parameter ω.
- Block variants of the above, such as alternating line Gauss–Seidel (ALGS).
- Pattern variants such as red–black or zebra relaxation. These exploit the structure of the stencil in order to avoid recursion in the algorithm and are therefore strong candidates in a parallel computing environment.
- Approximate inverse methods such as that of Frederickson [11].
- Incomplete decomposition schemes such as incomplete LU factorisation (ILU) [25].
- Preconditioned conjugate gradient methods; see [16].

This paper concentrates on ALGS and ILU, since these methods are thought most likely to deal effectively with anisotropy [15, 24]. The particular ILU method used allows non-zero entries in L and U only where they appear in $L^{(k)}$. To facilitate implementation of the multigrid algorithm on a parallel machine the ALGS could easily be replaced by alternating zebra (AZ), which is likely to perform at least as well as ALGS.

As explained in Section 5.1 the rôle of this iteration, in the context of multigrid, is to damp high frequency error components effectively. Existence of suitable smoothers is dependent on the discrete ellipticity of the approximation since no damping can generally be achieved at points in Fourier space where the symbol of $L^{(1)}$ vanishes. The investigation of discrete ellipticity in Section 4.3 suggests that smoothing methods do indeed exist for the current discretisation, as is borne out by the numerical experiments described below.

6. RESULTS

The following series of test problems are designed to establish the accuracy and stability of the new discretisation and to demonstrate the efficiency of the multigrid procedure in comparison to single grid methods using standard iterative schemes such as ALGS and ILU.

In the case of a diagonal permeability matrix, the discretisation presented above reduces to the standard one as used by Wesseling [27], where the accuracy of the scheme and the effectiveness of multigrid with ILU smoothing are demonstrated. All of the problems reported below involve full permeability matrices, and so are not covered by the methods of [27].

Results are presented in a number of ways. If true solutions are known the accuracy of the scheme is illustrated by presenting tables of error norms on increasingly refined meshes. The root mean square norm is used to define these. Second-order accuracy is therefore indicated by these norms quartering as the mesh steplength is halved. Multigrid algorithms always use $\nu_1 = 1 = \nu_2$, with $\gamma = 1$, unless otherwise stated. To assess convergence behavior the multigrid method is iterated until the l_2 norm of the residual is reduced by a factor 10^6. Various tables present the number of iterations required for convergence, and these are compared against the same values for the single grid method, which appear in parentheses. As an indication of the computational savings due to the multigrid acceleration total cpu time requirements are given for both single and multigrid experiments. These timings were measured on a Sun Spark 1 workstation. Contour plots of approximate solutions are also given for selected examples. In all cases these have been obtained using the mesh defined by (3.1), with $I = J = 128$.

6.1. *Problem 1: Constant Non-diagonal Permeability*

This test problem is designed to establish the accuracy of the discretisation for constant but non-diagonal permeability

TABLE I

Error Norms on Successively Refined Meshes: Problem 1

N	8	16	32	64	128
$\|e\|_2$	1.16E-3	2.89E-4	7.28E-5	1.83E-5	4.66E-6

TABLE III

Cpu Times Required for Various Smoothers

N	8	16	32	64	128
PGS	0.3 (0.3)	0.8 (2.3)	2.7 (23.4)	10.0 (313.3)	39.6 (4332.4)
ALGS	0.2 (0.3)	0.9 (2.1)	3.0 (26.7)	12.8 (378.4)	51.7 (5605.9)
ILU	0.2 (0.1)	0.5 (0.7)	2.0 (5.7)	7.7 (71.3)	30.2 (995.0)

matrices. The truncation error has already been found to be of second order in Section 4.2. If the method is sufficiently stable we therefore expect second-order global errors. The example also tests the effect of the off-diagonal terms on convergence of the single and multigrid methods, for various smoothers.

The region of solution is $\Omega = (0, 1)^2$. The permeability is defined by the positive definite matrix

$$K = \begin{pmatrix} 2 & 1 \\ 1 & 2 \end{pmatrix}, \tag{6.1}$$

and the true solution is $p = e^{xy}$. The root mean square error norms are presented in Table I, from which it is clear that second-order global accuracy has been achieved.

To facilitate comparison between the various smoothing methods, and between single and multigrid schemes, Tables II and III present the number of iterations required to reduce the residual norm by a factor of 10^6 and the cpu time taken, respectively. The values in parentheses refer to the single grid method. For this test problem the multigrid method achieves grid independent convergence rates, the most efficient method being ILU. This method also works best as a single grid iteration. Comparison with [27] shows that no significant degradation in convergence of either the single or multigrid methods is observed through the introduction of the mixed derivative term. The maximum speed-up due to multigrid on this sequence of meshes is 109 for point Gauss–Seidel (PGS), 108 for ALGS, and 33 for ILU.

Although the multigrid convergence rates obtained for this example are fast and mesh independent, the experimentally observed asymptotic value of the smoothing factor $\bar{\mu}$ for ALGS was only 0.471. This represents the effective residual norm reduction of each smoothing iteration within the multigrid. Smoothing analysis predicts a value of the smoothing factor

TABLE II

Number of Iterations Required for Various Smoothers

N	8	16	32	64	128
PGS	10 (75)	12 (272)	14 (987)	14 (3548)	15 (12593)
ALGS	6 (26)	7 (88)	7 (317)	8 (1146)	8 (4119)
ILU	3 (10)	4 (28)	5 (94)	5 (334)	5 (1207)

$\bar{\mu} = 0.159$, which is considerably smaller. Since the prediction of multigrid convergence rates from Fourier analysis is generally reliable, this suggests that the coarse grid correction is not completely effective at damping smooth error modes. Thus some changes to the definitions of the grid transfer and coarse grid operators might improve the convergence still further. Similar comments apply to the multigrid scheme with ILU smoothing, for which the observed rate was $\bar{\mu} = 0.211$ as opposed to the predicted value of $\bar{\mu} = 0.075$.

6.2. *Problem 2: Rotated Anisotropy*

In the important case where the permeabilities are represented by a diagonal matrix K, with $K_{xy} = 0$, the model problem (2.1) is said to be anisotropic if either $K_{xx} \ll K_{yy}$, or $K_{yy} \ll K_{xx}$. In the more general case $K_{xy} \neq 0$, the matrix K may be reduced to a diagonal matrix Λ by means of an orthogonal similarity transformation. Thus if K has the real eigenvalues λ_1 and λ_2, with corresponding orthogonal eigenvectors v_1, v_2, the diagonalisation may be written

$$K = R\Lambda R^T, \quad R = (v_1|v_2), \quad \Lambda = \begin{pmatrix} \lambda_1 & 0 \\ 0 & \lambda_2 \end{pmatrix}. \tag{6.2}$$

Defining canonical variables ξ, η by

$$\begin{pmatrix} \xi \\ \eta \end{pmatrix} = R^T \begin{pmatrix} x \\ y \end{pmatrix} \tag{6.3}$$

gives

$$\hat{\nabla} = \begin{pmatrix} \dfrac{\partial}{\partial \xi} \\ \dfrac{\partial}{\partial \eta} \end{pmatrix} = R^T \nabla, \tag{6.4}$$

and if the eigenvectors are independent of $\mathbf{x}$

$$\nabla \cdot w = \hat{\nabla} \cdot (R^T w), \quad w \in \mathbb{R}^2. \tag{6.5}$$

Thus

$$\nabla \cdot (K \nabla p) = \nabla \cdot (R\Lambda R^T R \hat{\nabla} p) = \hat{\nabla} \cdot (\Lambda \hat{\nabla} p) = f, \tag{6.6}$$

giving the canonical form

$$\frac{\partial}{\partial \xi}\left(\lambda_1 \frac{\partial p}{\partial \xi}\right) + \frac{\partial}{\partial \eta}\left(\lambda_2 \frac{\partial p}{\partial \eta}\right) = f. \tag{6.7}$$

Clearly anisotropy can occur in the direction of the eigenvectors of K if $\lambda_1 \ll \lambda_2$ or vice versa.

In this test problem the permeabilities remain constant, but are defined to give anisotropic problems at various angles. Line smoothers are clearly efficient if the anisotropy is aligned with the mesh, and the incomplete LU scheme can deal with these cases as well as anisotropy along mesh diagonals. The current problem tests the smoother's ability to deal with more general orientations of anisotropy. The definition is as for Problem 1, except that

$$K = \begin{pmatrix} c^2 + \varepsilon s^2 & (1-\varepsilon)sc \\ (1-\varepsilon)sc & s^2 + \varepsilon c^2 \end{pmatrix}, \quad c = \cos(\theta), s = \sin(\theta). \tag{6.8}$$

In the limit as $\varepsilon \to 0$ the partial differential equation reduces to the parabolic equation

$$\frac{\partial^2 p}{\partial \xi^2} = f, \tag{6.9}$$

where the variable ξ is constant along the line $\theta = \pi/2$.

In fact this problem represents the most general constant positive definite permeability, since the symmetry of K implies that it has real eigenvalues and orthogonal eigenvectors. These eigenvectors define orthogonal directions in which second derivatives may be taken, whilst the eigenvalues determine the anisotropy ratio. By suitable scaling of f any problem of the type (2.1), with constant K, can therefore be written in the form (6.8).

The results for incomplete LU and ALGS are represented in Fig. 5, with ε chosen as 10^{-10}, and for various angles θ. The numbers of multigrid iterations required are periodic, with period π; hence the upper half circle of Fig. 5 is used to give results for ILU, and the lower half circle gives results for ALGS. The concentric circles correspond to different degrees of mesh refinement, whilst the angle of a given radius defines θ.

As expected, if θ is a multiple of $\pi/2$ both methods are virtually direct, as they would be for a single grid scheme. For $\theta = \pi/4$, and as $\varepsilon \to 0$, the discrete approximation in the interior, given by (4.3), reduces to a three-point second difference along the relevant diagonal of the mesh. The ILU decomposition of this is exact. Hence convergence is very fast, and the method would be direct if it were not for the influence of the boundary conditions. However, at other angles, particularly in the first quadrant, ILU behaves erratically and may not always converge. This divergence was also observed in the single grid ILU method whenever it occurred with multigrid. One possible remedy to the divergence of ILU at certain angles would be to use two incomplete decompositions, with different point orderings. Unfortunately the storage requirements of such a scheme would generally be prohibitive.

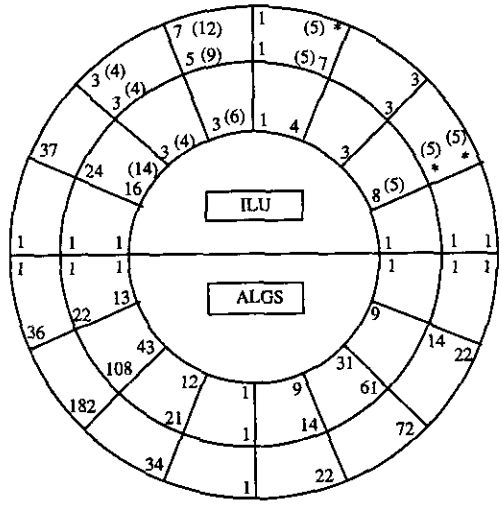

FIG. 5. Test problem 2: ILU and ALGS for rotated anisotropy. Number of multigrid iterations to convergence at various angles θ. Inner ring $I = J = 16$, middle ring $I = J = 32$, outer ring $I = J = 64$, $\varepsilon = 10^{-10}$, * denotes failure to converge. Figures in brackets denote iteration numbers of MILU, where they differ from those for ILU.

Another alternative is the use of modified versions of ILU, as investigated in [12, 22, 18, 17, 29], for example. In the notation of [28], the modification with parameter $\beta = 1$ was used. Where they differ from those for unmodified ILU, the numbers of iterations required are shown in brackets in Fig. 5. Smaller values of β were found not to be as robust. Clearly the problem of erratic convergence behaviour for standard ILU at certain anisotropy angles is solved by using the modified version of ILU.

The ALGS multigrid method was convergent for all angles tested, as was its single grid version. However, the convergence rates obtained were not mesh independent as can be seen from Fig. 5.

6.3. *Problem 3: Discontinuous Positive Definite Permeability Matrices, with Known Analytical Solutions*

Results for two test problems are presented in this section. Both have known analytical solutions and are designed to estimate experimentally the order of accuracy of the global error in the case of a discontinuous positive definite permeability matrix.

The first example, Problem 3a, is posed on $\Omega = (-1, 1)^2$, with K defined by

$$K = \begin{pmatrix} 1 & 0 \\ 0 & 1 \end{pmatrix}, \tag{6.10}$$

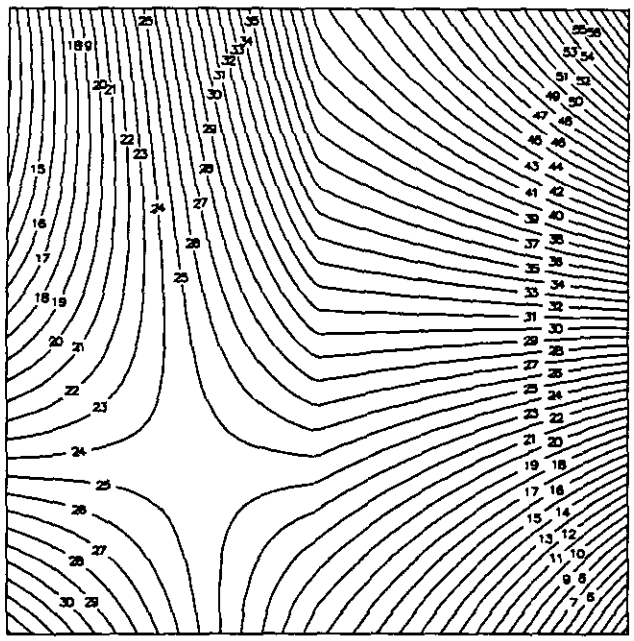

FIG. 6. Solution of test problem 3a.

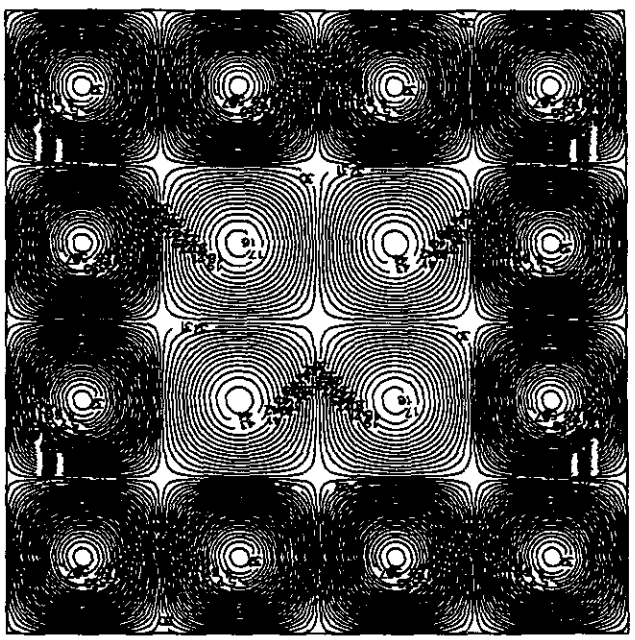

FIG. 7. Solution of sinusoidal test problem 3b.

for $x < 0$ and

$$K = \alpha \begin{pmatrix} 2 & 1 \\ 1 & 2 \end{pmatrix}, \tag{6.11}$$

for $x > 0$, where the parameter α is used to vary the strength of the discontinuity at $x = 0$. Dirichlet values are imposed on $\delta\Omega$.

The true solution is

$$p = \begin{cases} (2\sin(y) + \cos(y))\alpha x + \sin(y), & x < 0 \\ \exp(x)\sin(y), & x > 0 \end{cases}. \tag{6.12}$$

The approximate solution for $\alpha = 1$, $N = 128$ is shown in Fig. 6, whilst Table IV gives the root mean square error norms on a sequence of meshes. The method is clearly second-order accurate for this test problem.

TABLE IV

Error Norms on Successively Refined Meshes: Problem 3a

N	8	16	32	64	128
$\alpha = 1$	3.33E-3	9.37E-4	2.45E-4	6.25E-5	1.57E-5
$\alpha = 10$	1.64E-2	4.35E-3	1.11E-3	2.81E-4	7.04E-5
$\alpha = 100$	1.81E-1	4.74E-2	1.21E-2	3.04E-3	7.62E-4
$\alpha = 1000$	1.83E-0	4.79E-1	1.22E-1	3.07E-2	7.70E-3

The second example, Problem 3b, is defined on $\Omega = (-2, 2)^2$. The permeability is given by (6.11) for $\mathbf{x} \in \Omega_I = [-1, 1]^2$ and $K = I$ in Ω/Ω_I. Dirichlet conditions are specified on $\delta\Omega$. The true solution is

$$p = \begin{cases} \sin(\pi \mathbf{x})\sin(\pi y), & \mathbf{x} \in \Omega_I \\ 2\sin(\pi \mathbf{x})\sin(\pi y), & \mathbf{x} \in \Omega/\Omega_I. \end{cases} \tag{6.13}$$

Figure 7 shows the numerical solution. Table V presents error norms. Once again it is clear that second-order global accuracy is achieved. All results were obtained within seven multigrid iterations.

6.4. *Problem 4: Staircase Problem*

This is an example of a problem with discontinuous non-diagonal permeability, together with sources, sinks, and zero flux boundary conditions. The geometry of the problem is de-

TABLE V

Error Norms on Successively Refined Meshes: Problem 3b

N	8	16	32	64	128
$\|e\|_2$	2.43E-1	5.15E-2	1.20E-2	2.93E-3	7.26E-4

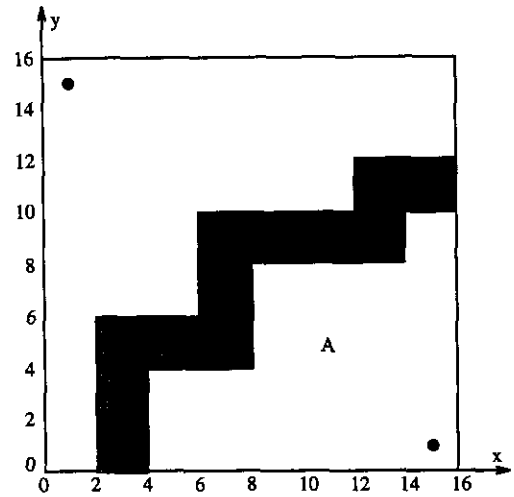

FIG. 8. *Geometry for staircase problem 4.*

fined in Fig. 8. A source of strength 1.0 was placed at (1, 15) and an equal and opposite sink at (15, 1). In region A the permeability is

$$K = \begin{pmatrix} 100 & 10 \\ 10 & 100 \end{pmatrix}, \tag{6.14}$$

whilst in region B it is

$$K = \begin{pmatrix} 1 & 2 \\ 2 & 5 \end{pmatrix}. \tag{6.15}$$

The approximate solution is shown in Fig. 9. This was found to be a relatively hard test problem, requiring 84 iterations of multigrid, using ALGS smoothing on a 128 × 128 mesh. The cpu time requirement was 383 s. Using ILU as a smoother the problem was solved in 28 multigrid iterations, which required 82 s of cpu time. A single grid ILU solver took 152,271 iterations to solve the same problem, at a cost of 121,712 cpu seconds. For this example the multigrid solution was therefore more than a thousand times faster.

6.5. *Problem 5: Generalised Stone's Problems*

The series of test problems discussed in this section are all modifications of Stone's third test problem from [25]. The region of solution is $\Omega = (0, 32)^2$ and the geometry is depicted in Fig. 10. Sources of strength 1.0, 0.5, and 0.6 are placed at (3, 3), (3, 27), and (23, 4), respectively. Sinks of strength -1.83 and -0.27 are placed at (14, 15) and (27, 27), respectively. Zero flux conditions are implemented on $\delta\Omega$. The permeability matrix is given by K_A in region A and so forth.

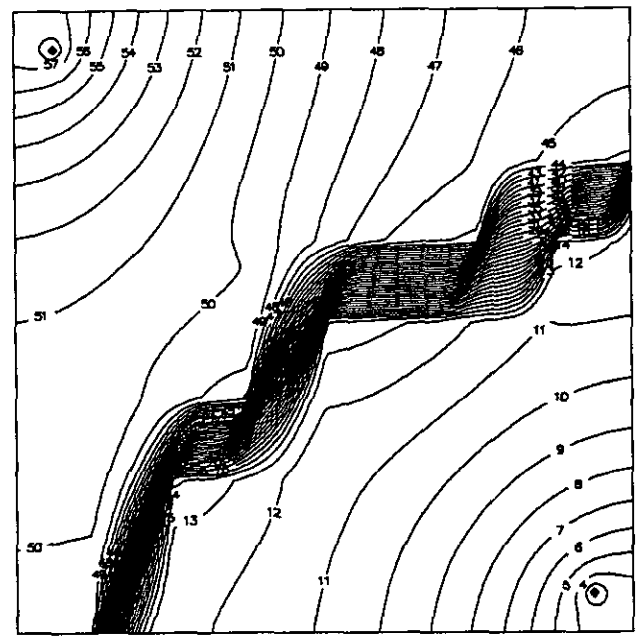

FIG. 9. Solution of staircase problem 4.

The first example is Stone's original problem (with slight modifications to the geometry), for which

$$K_A = \begin{pmatrix} 1 & 0 \\ 0 & 1 \end{pmatrix}, \quad K_B = \begin{pmatrix} 1 & 0 \\ 1 & 100 \end{pmatrix},$$
$$K_C = \begin{pmatrix} 100 & 0 \\ 0 & 1 \end{pmatrix}, \quad K_D = \begin{pmatrix} 0 & 0 \\ 0 & 0 \end{pmatrix}. \tag{6.16}$$

The first modification (M1) of this problem is obtained by

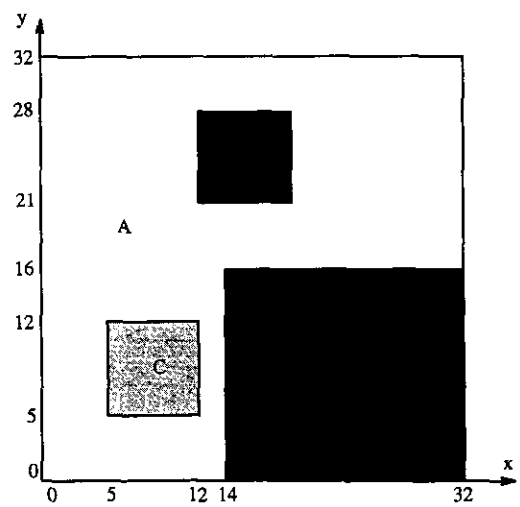

FIG. 10. Geometry for Stone's test problem.

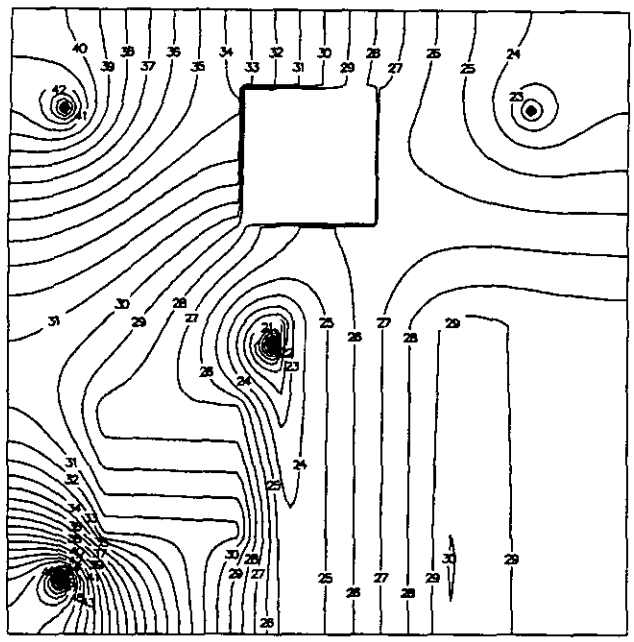

FIG. 11. Solution of Stone's test problem: M0.

replacing K_C by (6.11), whilst the second modification (M2) has K_A replaced by (6.11). The third modification (M3) is to replace K_C by

$$K_C = \begin{pmatrix} 25.75 & -42.87 \\ -42.87 & 75.25 \end{pmatrix}, \tag{6.17}$$

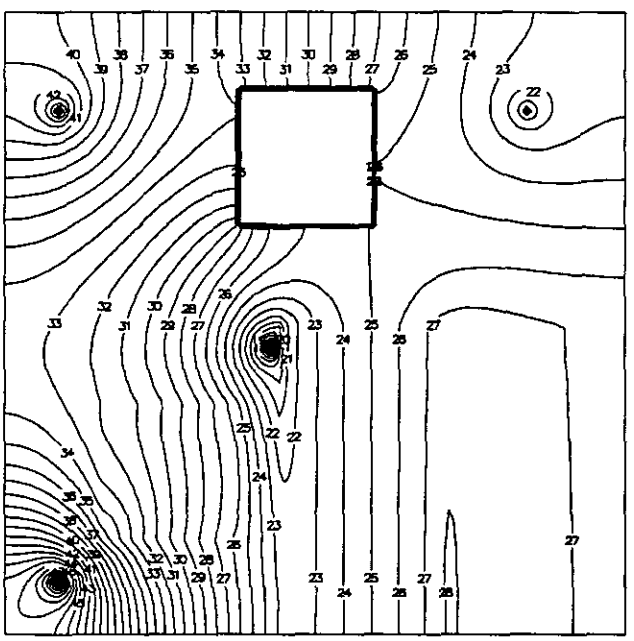

FIG. 12. Solution of first modification of Stone's problem: M1.

TABLE VI

Stone's Problem and Its Modifications

N^a	32	64	128	N^b	32	64	128
M0	11	12	13	M0	2.8	11.4	46.6
M1	8	10	12	M1	2.3	10.0	47.6
M2	10	14 (14091)	20	M2	2.8	13.0 (2811.1)	65.6
M3	9	9	9	M3	5.2	20.7	83.7

Note. M0, Stone's problem; M1, modification 1; M2, modification 2; M3, modification 3.

[a] Number of iterations.

[b] Cpu times required for multigrid with ILU smoothing.

corresponding to anisotropy of strength 100 aligned at 120° to the x axis.

Numerical solutions for Stone's problem and its three modifications are shown in Figs. 11–14. Table VI shows the number of iterations and cpu times required for convergence, for multigrid with ILU smoothing, whilst Table VII presents the same results with ALGS smoothing. For the third modification M3, the results are for modified ILU with W-cycle multigrid, with $\nu_1 = \nu_2 = \gamma = 1$; unmodified ILU failed to converge for the restriction (5.8), although it did solve the problem efficiently with the restriction (5.11). The rates for multigrid with ILU smoothing are virtually mesh independent. For M2 with $N = 64$, a speedup of over 200 over the single grid method was obtained.

The method using ALGS as a smoother is less efficient than the ILU scheme and has convergence rates which deteriorate slightly as the mesh is refined. However, once again the multigrid scheme gives significant reductions in CPU time, a speedup of 151 was achieved for ALGS applied to the problem mentioned above.

7. CONCLUSIONS

A cell-centred finite volume discretisation of the pressure equation arising in an IMPES reservoir simulation has been

TABLE VII

Stone's Problem and Its Modifications

N^a	32	64	128	N^b	32	64	128
M0	85	103	119	M0	20.3	96.6	445.2
M1	46	56	65	M1	11.0	51.6	262.8
M2	63	76 (40205)	88	M2	16.0	73.7 (11149.8)	351.7
M3	115	144	172	M3	27.4	130.3	650.6

Note. M0, Stone's problem; M1, modification 1; M2, modification 2; M3, modification 3.

[a] Number of iterations.

[b] Cpu times required for multigrid with ALGS smoothing.

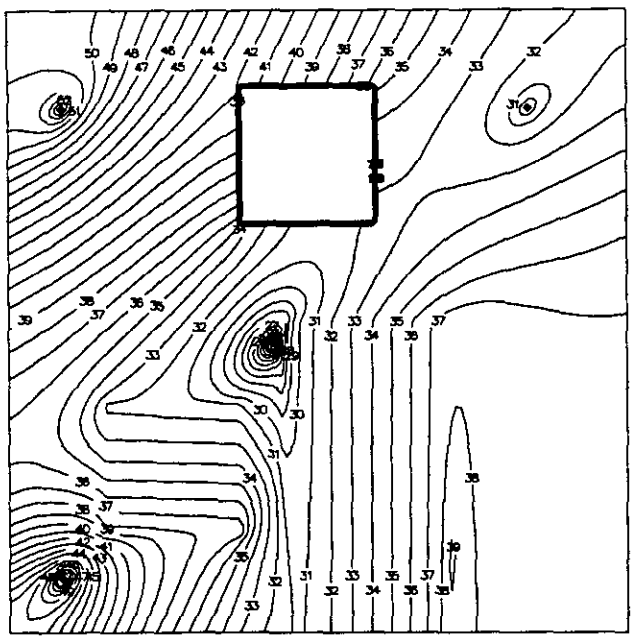

FIG. 13. Solution of second modification of Stone's problem: M2.

presented. This discretisation is suitable for problems in which the permeabilities are heterogeneous and represented by a non-diagonal matrix, with strong discontinuities. It has been shown to achieve second-order global accuracy for several test problems with known solutions. The method reduces to a well-known scheme in the case of a diagonal permeability matrix and can be trivially applied to a non-uniform structured mesh.

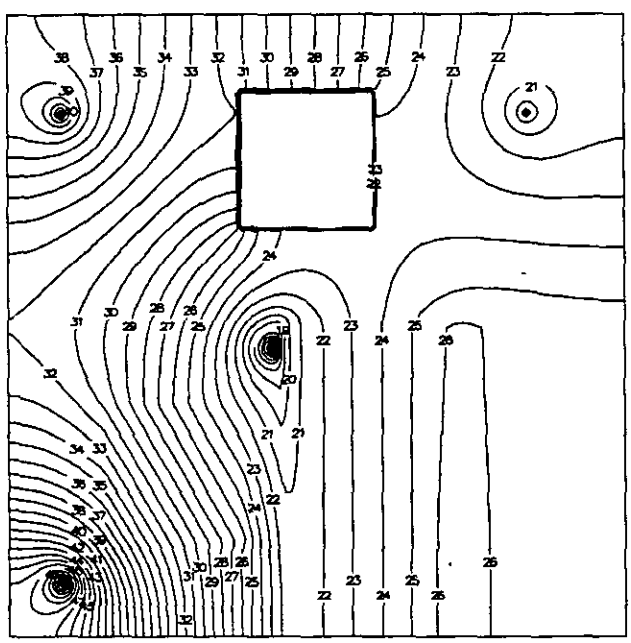

FIG. 14. Solution of third modification of Stone's problem: M3.

Thus it enables accurate treatment of a much wider class of problems than by methods previously discussed in the literature. The approach may also be extended to three dimensions.

An efficient and robust multigrid procedure has been used to solve the algebraic equations derived using the method. This gave substantial cpu time savings over a single grid method for all test problems considered. Effectively grid-independent convergence rates were achieved for a range of test cases with strongly discontinuous non-diagonal permeability matrices, including several generalisations of Stone's problem.

REFERENCES

1. R. Alcouffe, A. Brandt, J. Dendy, and J. Painter, *SIAM J. Sci. Stat. Comput.* **2,** 430 (1981).
2. K. Aziz and A. Settari, *Petroleum Reservoir Simulation* (Appl. Sci., London, 1979).
3. R. E. Bank and C. C. Douglas, *SIAM J. Numer. Anal.* **22,** 617 (1985).
4. A. Behie and P. Forsyth, *Soc. Pet. Eng. J.* **23,** 623 (1983).
5. A. Behie and P. Forsyth, *Appl. Math. Comput.* **13,** 229 (1983).
6. A. Brandt, *Math. Comput.* **31,** 333 (1977).
7. P. de Zeeuw, *J. Comput. Appl. Math.* **33,** 1 (1990).
8. J. Dendy, *Appl. Math. Comput.* **13,** 261 (1983).
9. J. E. Dendy, *SIAM J. Sci. Stat. Comput.* **8,** 673 (1987).
10. J. Dendy, S. McCormick, J. Ruge, and T. Russell, *Multigrid Methods for Three-Dimensional Petroleum Reservoir Simulation,* SPE Paper 18409, 1989, in the *SPE Symposium on Reservoir Simulation in Houston, TX, February 6–8* (unpublished).
11. P. Frederickson, *Fast Approximate Inversion of Large Elliptic Systems,* Tech. Rep. 7-74, Lakehead University, 1974 (unpublished).
12. P. W. Hemker, *The Incomplete LU-Decomposition as a Relaxation Method in Multi-grid Algorithms* (Boole Press, Dublin, 1980), p. 306.
13. M. Hestenes and E. Stiefel, *J. Res. Nat. Bur. Stand.* **49,** 409 (1952).
14. D. Kershaw, *J. Comput. Phys.* **26,** 43 (1978).
15. R. Kettler, Analysis and comparison of relaxation schemes in robust multigrid and preconditioned conjugate gradient methods, in *Multigrid Methods: Proceedings, Conference, Koln-Porz,* edited by W. Hackbusch and U. Trottenberg. Lecture Notes in Math, Vol. 960 (Springer-Verlag, Berlin, 1981).
16. R. Kettler and J. Meijerink, *A multigrid method and a combined multigrid–conjugate gradient method for elliptic problems with strongly discontinuous coefficients in general domains,* Shell Pub. 604, (KSEPL, Rijswijk, 1981).
17. M. Khahil, *Analysis of Linear Multigrid Methods for Elliptic Differential Equations with Discontinuous and Anisotropic Coefficients,* Ph.D. thesis, Delft University of Technology, 1989 (unpublished).
18. M. Khahil, *Local Mode Smoothing Analysis of Various Incomplete Factorisation Iterative Methods,* Notes on Numerical Fluid Mechanics, Vol. 123 (Viewig, Braunschweig, 1989), p. 155.
19. K. Khalil and P. Wesseling, *J. Comput. Phys.* **98,** 1 (1992).
20. P. King, *Transp. Porous Media* **4,** 37 (1989).
21. J. Meijerink and H. van der Vorst, *Math. Comput.* **31,** 148 (1977).
22. K. D. Oertel and K. Stüben, Multigrid with ILU smoothing—Systematic tests and improvements, Notes on Numerical Fluid Mechanics, Vol. 123, (Viewig, Braunschweig, 1989), p. 188.
23. D. Peaceman and H. Rachford, *J. Soc. Indus. Appl. Math.* **3,** 28 (1955).

24. P. Sonneveld and P. Wesseling and P. M. de Zeeuw, Multigrid and conjugate gradient methods as convergence acceleration techniques, in *Multigrid Methods for Integral and Differential equations: Proceedings, Conference, Bristol,* edited by D. J. Paddon and H. Holstein, eds., Clarendon Press, Oxford, 1981.
25. H. Stone, *SIAM J. Numer. Anal.* **5,** 530 (1968).
26. P. Vinsome, *Orthomin, an Iterative Method for Solving Sparse Sets of Simultaneous Linear Equations,* SPE Paper 5729, 1976; in *Fourth Symposium on Numerical Simulation of Reservoir Performance, Los Angeles, Feb. 19–20, 1976* (unpublished).
27. P. Wesseling, *J. Comput. Phys.* **79,** 85 (1988).
28. P. Wesseling, *An Introduction to Multigrid Methods* (Wiley, Chichester, 1992).
29. G. Wittum, *SIAM J. Sci. Stat. Comput.* **10,** 699 (1989).
30. D. Young, *Iterative Solution of Large Linear Systems* (Academic Press, New York, 1971).